Proceedings of the IASS 2024 Symposium
Redefining the Art of Structural Design
August 26-30, 2024, Zurich Switzerland
Philippe Block, Giulia Boller, Catherine DeWolf,
Jacqueline Pauli, Walter Kaufmann (eds.)

Robot supported Wire Arc Additive Manufacturing – Using dot-by-dot printing for lattice column structures

Benedikt WALDSCHMITT*, Jörg LANGE

* Institute for Steel Construction and Materials Mechanics, Technical University of Darmstadt
Franziska-Braun-Straße 3, 64287 Darmstadt, Germany
waldschmitt@stahlbau.tu-darmstadt.de

Abstract

Wire Arc Additive Manufacturing (WAAM) is a robot-controlled welding process used to build up three-dimensional structures in steel. Like other Additive Manufacturing (AM) technologies, Wire Arc Additive Manufacturing (WAAM) allows for geometrically-complex structures to be manufactured which may be unfeasible to manufacture using conventional methods. In recent years, WAAM has also gained prominence in the fields of architecture and civil engineering, with applications ranging from fully-printed steel bridges to individualized steel components. This paper presents a workflow from material testing to manufacturing and destructive testing of lattice structures of various shapes and grids printed with a dot-by-dot welding process. In a first step, the WAAM-process, dot-by-dot printing and applicable cooling methods for vertical and cantilever struts are presented. 18 as-built struts, with vertical and 45° inclined build direction, are produced to provide a statement on the manufacturability of struts for lattice structures using dot-by-dot printing. The process stability, the susceptibility to welding defects and the geometric properties of the printed layers are analyzed. The struts are then tested for their material properties. Parametric robot programming is then used for the manufacturing process in order to realize various free-form column geometries. Finally, a destructive testing of as-built structures provides a statement on the load bearing capacity and thus the suitability for future use in the additive manufacturing of complex lattice column structures.

Keywords: metal spatial structures, lattice columns, Wire Arc Additive Manufacturing, Additive Manufacturing, dot-by-dot printing, parametric robot programming

1. Introduction

In contemporary architectural endeavours, buildings not only fulfil functional necessities but also serve as representatives of societal ideals and aspirations. The imperative for architectural innovation mandates a departure from standardized approaches, necessitating the integration of bespoke structures alongside conventional elements. Although modern steel fabrication techniques allow for some degree of customization, the process remains laborious, costly, and time intensive. Moreover, the escalating scarcity of skilled labour underscores the imperative for increased automation within the industry. Despite the prevailing reliance on traditional fabrication methods, the advent of Additive Manufacturing (AM) heralds promising prospects for the sector, particularly in terms of individualization and automation across diverse applications [1]. However, AM has not yet fully established itself in steel construction. While additive manufacturing with wire arc additive manufacturing (WAAM) focuses primarily on continuous welding processes, the feasibility and efficiency of dot-by-dot applications with WAAM should be investigated further. These are particularly suitable for the manufacturing of slender steel lattice structures. These innovative structures, exemplary illustrated in Figure 1 are characterized by their high load-bearing capacity, low weight and architectural versatility [2]. This paper explores the application of dot-by-dot printing for lattice structure manufacturing, illustrating the complexe process

Figure 1: Steel lattice structures a) Radio tower, Moscow [3]; b) King's Cross station, London; c) Swiss Re Building, London

and addressing critical gaps in material behavior understanding. It outlines the manufacturing process of initial lattice columns, highlighting challenges encountered. The study concludes with a structural tests of various column cross-sections, offering insights to enhance Wire Arc Additive Manufacturing (WAAM) potential in the steel construction industry.

2. Wire Arc Additive Manufacturing

2.1. Process description

Within the steel construction industry, the research in WAAM has raised attention. WAAM is an additive manufacturing process based on gas shielded metal arc welding (GMAW). The electric arc (mostly short arc and spray arc) melts the welding wire which serves as the printing material. The liquid molten pool solidifies in lines or spots which can be classified as continuous or discrete (also known as point-by-point or dot-by-dot welding) and forms three-dimensional structures. The shielding gas protects the material deposition from atmospheric influences and impurities. At the same time, it stabilizes the heat input of the welding process and influences the molten pool [4]. The degree of viscosity, the length and kind of active and passive cooling and thus the solidification process are decisive for the geometric shape of the seam, the target geometry and the material characteristics. The selection of the wire electrode significantly determines the material characteristics of the manufactured structure. Six-axis robotic systems, like the one at the laboratory of the Technical University of Darmstadt, given in Figure 2, for guiding the welding torch offer great flexibility in the manufacturing of components and are used to ensure production in large installation spaces. With increasing size, accuracy decreases as the distance to the machine origin extends [5]. To avoid inaccuracies large structures might be divided in segments to be manufactured simultaneously. At the same time, WAAM offers higher deposition rates compared to other metallic additive manufacturing processes and investment costs for supplies and system technology are significantly lower [6]. These aspects make the process attractive for the manufacturing of large structural components like free form steel lattice columns and its single components.

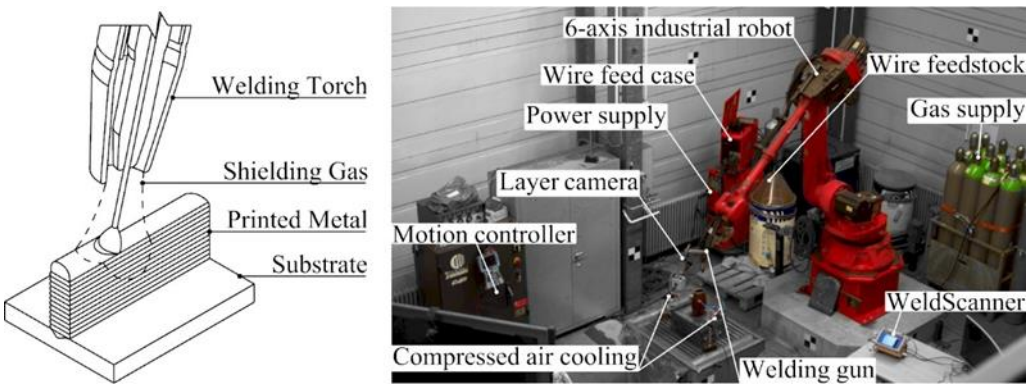

Figure 2: a) Material deposition of continuous welding in detail; b) WAAM-system at TU Darmstadt

2.2. Dot-by-dot printing

In contrast to the traditional method of layer-by-layer deposition to form solid structures, dot-by-dot printing represents a discrete material deposition process used in WAAM. This approach necessitates an intermediate cooling interval between successive layers to facilitate the solidification of each deposited droplet. Initial applied in the manufacturing of self-supporting bars for use as linear reinforcements in concrete structures [7–9], as well as to join non-touching parts during the assembly of steel elements [10], it has also found utility in the creation of lattice structures [11, 12]. Recent efforts have focused on refining process parameters and path-planning strategies [11, 13] Furthermore, investigations into the material behaviour of dot-by-dot printed structures utilizing mild carbon steel wire electrodes (ER70S-6) with wire diameters ranging from 0.8 mm to 1.2 mm and using shielding gases M21 and Ar85C14 have been undertaken. These studies, conducted using the welding process Cold Metal Transfer (CMT) and CMT Cycle Step, aim to determine the mechanical properties, including strength and elongation properties, of the resulting materials [7–9, 14]. Similar analyses were also carried out with the stainless steel ER 308LSi [11].

2.3. Cooling methods for WAAM

Within the domain of Wire Arc Additive Manufacturing, the cooling phase stands out as a pivotal determinant influencing both, manufacturing efficiency and process stability. Natural cooling processes, predominantly through heat radiation (NC = Natural Cooling) and heat flux into the component, inherently exhibit sluggish cooling rates. Consequently, researchers have embarked on exploring alternative cooling strategies aimed at accelerating the solidification process. Notably, investigations have been conducted to evaluate the efficacy of using water baths to hasten cooling kinetics and enhance overall productivity [15, 16]. Furthermore, there is a discernible shift towards the adoption of compressed air cooling (AC) or compressed air-aerosol mixtures (WAC) within the WAAM paradigm. This approach requires a differentiated cooling concept that includes stationary cooling intervals between successive welding layers [16–18] or AC or WAC cooling following the welding torch [16, 19]. The strategic deployment of these cooling mechanisms assumes paramount importance in regulating the interlayer temperature - a critical parameter described in EN ISO 13916-2017. This characteristic value characterizes the temperature gradient between successive welding layers immediately before the start of the welding process for the subsequent layer. Such careful temperature control is crucial for the design of the seam geometry and the material properties as part of the additive manufacturing process. Prior investigations into the utilization of different wire electrodes have yielded promising results, with limited discernible adverse effects on material properties, particularly when coupled with compressed air cooling or compressed air-aerosol mixtures [15, 17, 18]. These research findings highlight the compatibility and effectiveness of these cooling methods in mitigating potentially harmful effects on material integrity, supporting the case for their further integration into the WAAM framework.

3. Manufacturing of single dot-by-dot struts and lattice structures

While continuous welding is a fairly well-known process, discrete spot-by-spot welding follows some slightly different steps for depositing a droplet of material on an already solidified layer. To deposit the material, each iteration follows the repetitive actions shown in Figure 3. First, the robot moves to the target center point on the surface of the previous layer to achieve a constant CTWD (contact tip to work distance) of 12 mm, followed by a gas pre-flow phase to ensure protection from atmospheric influences. The arc is then ignited. While the arc process is running, the robot remains in position for a defined welding interval (dwell time) to achieve the desired vertical build-up direction until the arc process ends. While the weld pool is still solidifying, the gas post-flow still covers the weld seam. After several welding intervals, the height of the strut is measured using the TouchSense method offered by Fronius to determine the respective layer height. The measurement interval also provides sufficient time for each strut to cool naturally or by actively utilizing the cooling methods. An interlayer temperature of less than 150 °C was achieved (checked with a pyrometer every 5 layers), which proved to be favorable for process stability and material properties. The first two layers are recorded in scope mode (high-frequency recording rate of 3200 Hz) with a WeldScanner P1000 DV 25 GAS30l10b from HKS in order

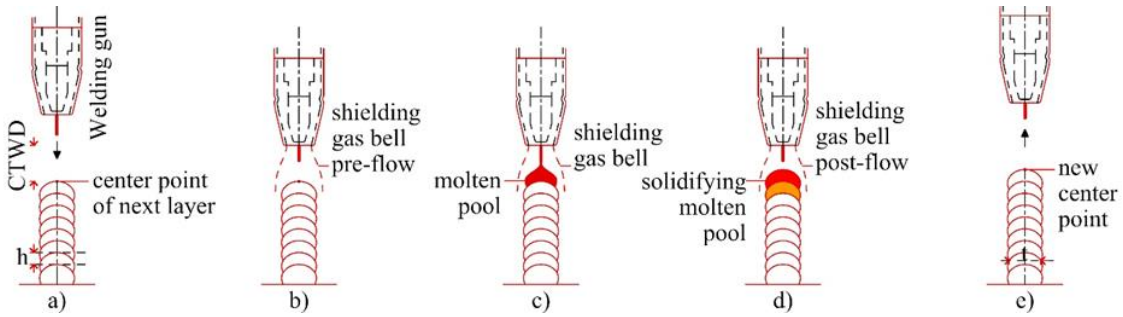

Figure 3: Principal illustration of material deposition interval for dot-by-dot printing

to be able to make a statement about the diameter of the manufactured single struts, they are measured in the notches evenly distributed over the height using a caliper gauge.

4. Process and Input parameters

The effectiveness of the material deposition in a stable welding process depends primarily on the careful selection and optimization of the welding and input parameters. These parameters have a major influence on the geometric properties of the weld seam and the resulting material properties. The wire feed speed, the specified travel speed of the robot system in continuous welding or the dwell time in spot-to-spot printing are essential components of this process control. The Cold Metal Transfer (CMT) process control, an energy-efficient welding technology developed by Fronius, is central to controlling the welding parameters. Table 1 shows the welding parameters of a Fronius CMT Advanced 4000 R welding source, which is equipped with the process variant CMT Cycle Step, that enables precise control of the material deposition. In addition, the relevant process parameters are described to provide a comprehensive understanding of the welding process. A dwell time of 0.7 seconds and a wire feed speed of 6.0 m/min is used for point material deposition. Given the documented influence of gas mixture on the geometric attributes of welded seams [20], the shielding gas C6X1 is used. To speed up the manufacturing process three cooling methods are tested to determine their advantageous and disadvantageous influences.

Table 1: Process and input parameters for the manufacturing of lattice structures

Process and input parameters	Variable	CMT Cycle Step Unit
Welding characteristic		1840
Number of CMT-Cycles	25	
Pause time	100	Ms
Wire-Feed-Speed (set)	6.0	m/min
Welding interval (set)	0.7	S
Wire electrode	Weko 2 G3Si1 (ER 70S-6) Ø 1.0 mm	
Shielding Gas	C6X1 (93 % Argon, 6 % CO_2, 1 % O_2) 15 l/min (pre-flow 1.2 s; post-flow 1.0 s)	
Welding torch orientation	0° to the vertical (neutral)	
CTWD (Contact tip to work distance)	12	Mm
Cooling method	WAC	Water + Air pressure cooling
	AC	Air pressure cooling
	NC	Natural cooling

5. Tensile testing of as-built struts

5.1. Manufacturing of tensile struts

For an investigation of the material properties, nine vertical struts and nine struts cantilevered at an angle of approximately 45°, shown in Figure 4, with a length of over 175 mm were manufactured for macrostructural investigations using as-built tensile tests. The key manufacturing parameters and recorded data are given in Table 2. NC, AC and WAC cooling were used for each series, resulting in

different cooling times. The target interlayer temperature of 150 °C was not always achieved, particularly for the vertical components, as the specified cooling time was set too short. The cantilevered struts have a lower height (measured in the vertical direction) and a smaller dot diameter and therefore a smaller cross-sectional area (measured in the longitudinal direction of the sample). In addition, fewer welding points are required to achieve the desired total length of at least 170 mm. Over 2600 spots were welded during the manufacturing of the struts. Defects occurred in less than 1.8 % of the layers, with less than 0.2 % of all layers showing structural weakening due to pores or weld interruptions, for example. This indicates a high level of process stability for the production of lattice columns.

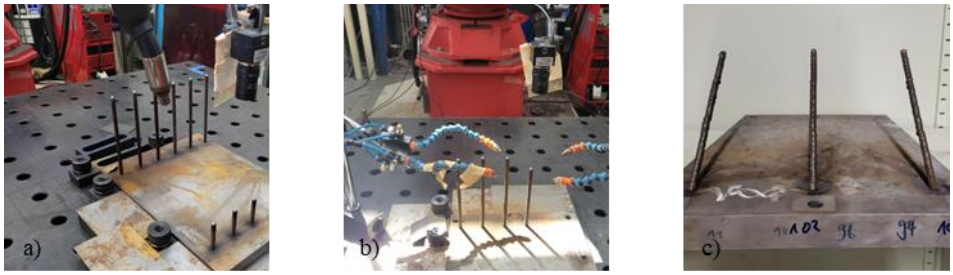

Figure 4: Manufacturing struts a) parallely using natural cooling; b) individually using AC; c) manuf. cantilevered struts

5.2. Test-set-up

The tests were carried out in a MAN 1000 kN hydraulic universal testing machine (UT), which is shown in Figure 7. The readings of load and displacement were recorded by the UT at a rate of 0.5 Hz. The UT was set to displacement control at a rate of 1.2 mm/min and the specimens were loaded in tensile beyond the ultimate load until the point of fracture was reached. Table 2 lists the specific height of each strut and as well as the average and minimum thickness (which are given exemplary with the white mark in Figure 5 b) and c) measured in the area of interest. The minimum value is used to calculate the stress values with the minimal cross-section area calculated with the circular cross-section. Figure 6 illustrates the stress-strain-curves of the tested specimens divided into the vertical and cantilevered deposition directions. The strains were determined at strains < 4.5 % using a touching extensometer with sharp callipers over the predefined initial gauge length. Strains > 4.5 % are measured using the machine path of the universal testing machine, so that these strains are only qualitatively meaningful. The fracture strain was determined on the destroyed samples in accordance with DIN EN ISO 6892-1 Eq. 6.

5.3. Evaluation of as-built tensile struts

The results of the tensile testing are given as stress-strain-curves in Figure 6 and enumerated in Table 3. For both deposition directions, the natural cooled specimens exhibit the lowest yield and ultimate strength. For T-RB-1 and T-RB-7, even the specified minimum yield strength value of 420 N/mm², given by the electrode manufacturer, is undershot. While the highest material strengths can be achieved for the vertical printing direction for WAC, the difference between AC and WAC is very small for the cantilevered ones. The results scatter in the range of approximately ± 0.4 to 4.8 % in particular for the test series T-RB-1. It should be noted that the results are based on the assumption of a circular cross-sectional area based on the minimum diameter. As a result, deviations from the actual stress in the cross-section may occur. Information on the modulus of elasticity will follow the evaluation of DIC results. Nevertheless, the material stiffness shows similar behaviour for the linear-elastic strain range. A ductile deformation behavior is obtained for all test specimens. The measured fracture length shows a very

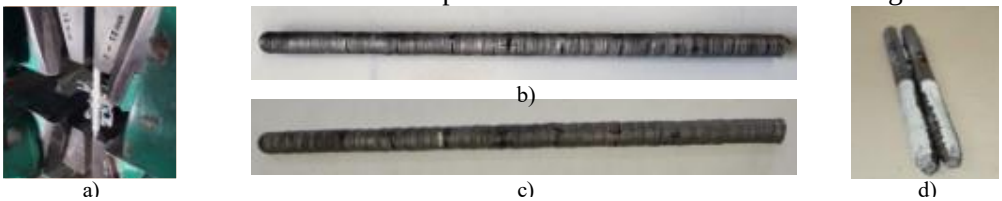

Figure 5: a) Test set-up; b) and c) manufactured struts; d) tensile tested strut

homogeneous result at approx. 25 % for the vertical deposition direction, while the elongation for the cantilevered struts is reduced to approx. 19 % for T-RB-7. One specimen T-RB-8 respectively did not fail in the gauge area but also showed no weakening due to structural inhomogeneities like pores. Compared with previous tests on mild carbon steel as-built tensile specimens [7–9, 14] which were mostly manufactured using CMT, higher material values were achieved for the yield strength and ultimate strength. In addition, the cooling approach seems to be beneficial regarding material strength, which allows to decrease manufacturing time.

Table 2: Details on manufacturing the as-built struts for macrostructural tensile testing

Test series		T-RB-1	T-RB-2	T-RB-3	T-RB-7	T-RB-8	T-RB-9
∑ specimens		3*	3**	3**	3*	3***	3***
Welding and process parameters							
Wire diameter	in mm	1.00				1.00	
Shielding gas		C6X1				C6X1	
Welding process		CMT CS				CMT CS	
$WFS_{parameter,measured}$	in m/min	6.2 (set 6.0)				6.2 (set 6.0)	
$t_{welding,set}$	in s	0.70				0.70	
$t_{welding,measured}$	in s	3.21	3.23	3.23	3.21	3.13	3.31
Cooling methode		NC	AC	WAC	NC	AC	WAC
Cooling time	in s	79 ± 1	25 ± 10	25 ± 10	118 ± 6	47 ± 6	59 ± 16
∑ layer		459	468	465	405	405	405
$E_{droplet}$	in kJ	2.13	2.14	2.15	2.17	2.14	2.12
$T_{interlayer}$***	in °C	281 ± 74	260 ± 61	210 ± 62	122 ± 62	48 ± 14	49 ± 14
Geometric properties and related parameter information							
$h_{layer,parameter}$	in mm	1.26 ± 0.25				0.9 - 1.0	
$h_{layer,specimen}$	in mm	1.180	1.181	1.168	0.954	0.945	0.951
$h_{specimen}$	in mm	17.77	17.74	17.67	-	17.82	18.10
$t_{parameter}$	in mm	7.52 ± 0.08				7.00 ± 0.09	
$t_{average}$****	in mm	7.76	7.77	7.76	7.34	7.08	7.09
t_{stddev}****	in mm	0.19	0.17	0.17	0.24	0.16	0.16
t_{min}****	in mm	7.49	7.43	7.41	7.02	6.87	6.88
A_{min}*****	in mm²	44.02	43.32	43.09	38.70	37.07	37.18
Process errors and failures affecting the structural integrity (absolute in percentage)							
Slaghammer		0 0.0%	4 0.9%	0 0.0%	2 0.4%	2 0.4%	0 0.0%
Ignition error		0 0.0%	2 0.4%	0 0.0%	0 0.0%	1 0.2%	0 0.0%
Welding interruption		2 0.4%	1 0.2%	1 0.2%	0 0.0%	0 0.0%	0 0.0%
Incomplete Cycle		0 0.0%	1 0.2%	0 0.0%	0 0.0%	0 0.0%	0 0.0%
Pores		0 0.0%	0 0.0%	0 0.0%	0 0.0%	0 0.0%	0 0.0%
layer repeated		2 0.4%	3 0.7%	2 0.4%	21 4.6%	0 0.0%	3 0.7%
offgassing		0 0.0%	0 0.0%	0 0.0%	0 0.0%	0 0.0%	0 0.0%
burn-back		0 0.0%	0 0.0%	0 0.0%	0 0.0%	0 0.0%	0 0.0%
Wire stick		0 0.0%	0 0.0%	0 0.0%	0 0.0%	0 0.0%	0 0.0%
		T-RB-1a	T-RB-2a	T-RB-3a	T-RB-7a	T-RB-8a	T-RB-9a
		T-RB-1b	T-RB-2b	T-RB-3b	T-RB-7b	T-RB-8b	T-RB-9b
		T-RB-1c	T-RB-2c	T-RB-3c	T-RB-7c	T-RB-8c	T-RB-9c

* 3 specimens were manufactured parallely

** each specimen was manufactured individually

*** 2 specimens were manufactured parallely

**** data provided for the area of interest/tested

***** calculated as circular cross section based on the thickness t_{min}

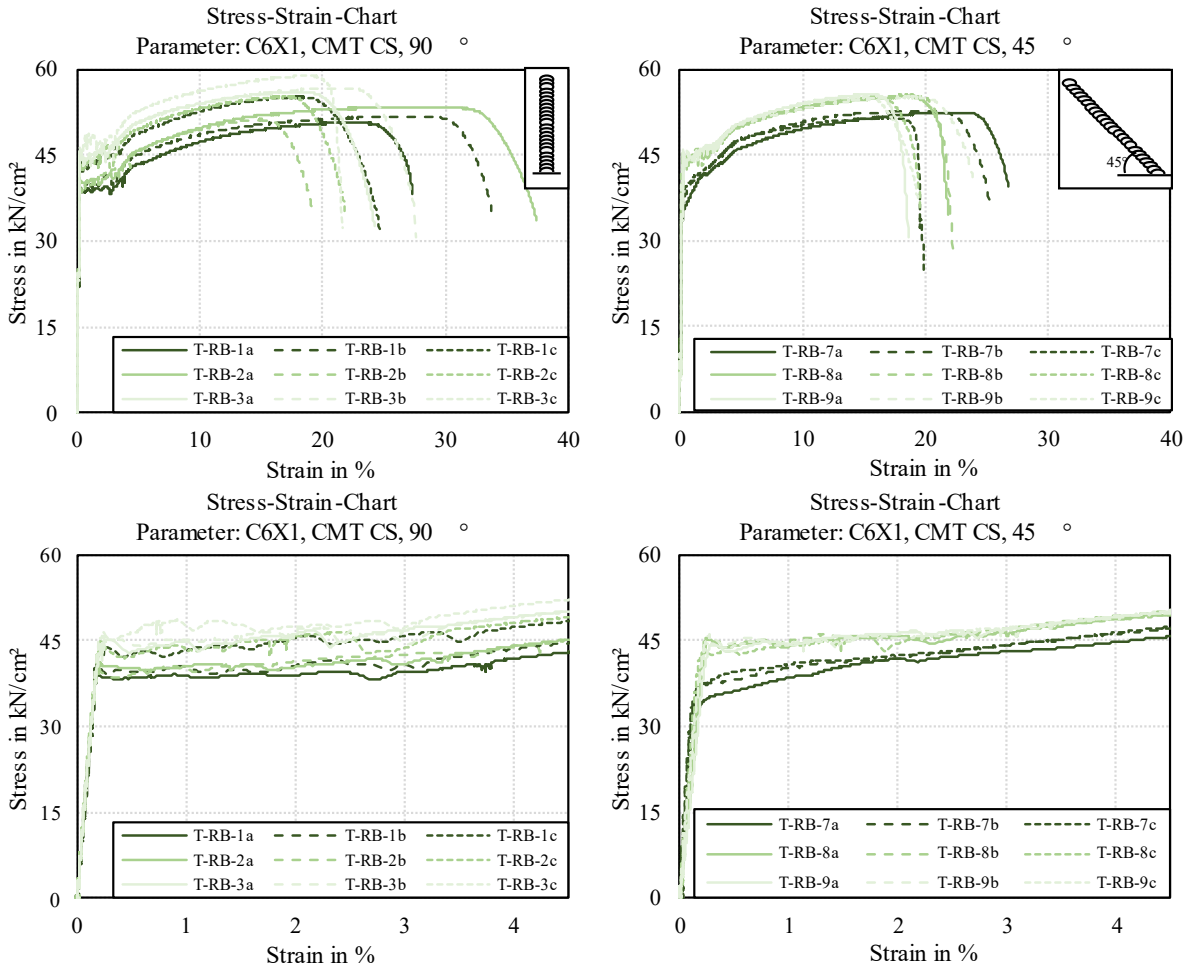

Figure 6: Stress-strain curves of dot-by-dot printed vertical and cantilevered struts using different cooling methodes

Table 3: Resulting strength and fracture of strain for as-built dot-by-dot printed vertical and cantilevered struts

Test series		T-RB-1	T-RB-2	T-RB-3	T-RB-7	T-RB-8	T-RB-9
Mean Area	in mm²	47.336	47.381	47.250	42.314	39.369	39.480
Min. Area	in mm²	44.022	43.319	43.086	38.705	37.068	37.176
$Load_{yield\ strength}$	in kN	8.9	9.4	10.4	9.5	12.0	12.1
Upper yield strength	in N/mm²	391 ± 7	406 ± 15	449 ± 9	369 ± 10	444 ± 12	449 ± 8
Tensile strength	in N/mm²	525 ± 25	533 ± 17	572 ± 12	522 ± 5	552 ± 2	552 ± 2
Fracture strain	in %	27 ± 4	26 ± 3	25 ± 2	19* ± 2	22 ± 2*	27 ± 2

* at least one specimen not in the initial gauge length

6. Lattice column structures

6.1. Additive manufacturing

Eight structures of different lattice column shapes were manufactured in pairwise segments for vertical and cantilevered struts (Figure 7 a)). Table 4 lists the relevant manufacturing information. Seven columns were manufactured with a constant outer radius (straight) and one with a parabolic view (parabolic). For comparison, seven columns were manufactured with a hexagonal lattice structure and one column with a diamond-shaped pattern (consisting only of diagonal struts). Figure 7 c) shows the different patterns. The welding trajectories of the various struts were generated based on Parametric Robot Programming (PRP), whereby the x and y coordinates are calculated by mathematical functions using the current structure height, column radius and grid width [21]. After being manufactured, the columns are sandblasted and welded to second plate arranged parallel to the base plate and installed in

the test setup (Figure 7 d)). The column diameter is 60 mm. A total of 16056 welding points were applied during manufacturing all columns with a welding error percentage of 0.38 %. The different layer heights of 1.30 mm (vertical) and 1.21 mm (diagonal) had to be taken into account in the robot trajectory determination. At a length less than 50 mm, the struts are not in the stability-endangered range, so that a full load-bearing capacity is assumed here.

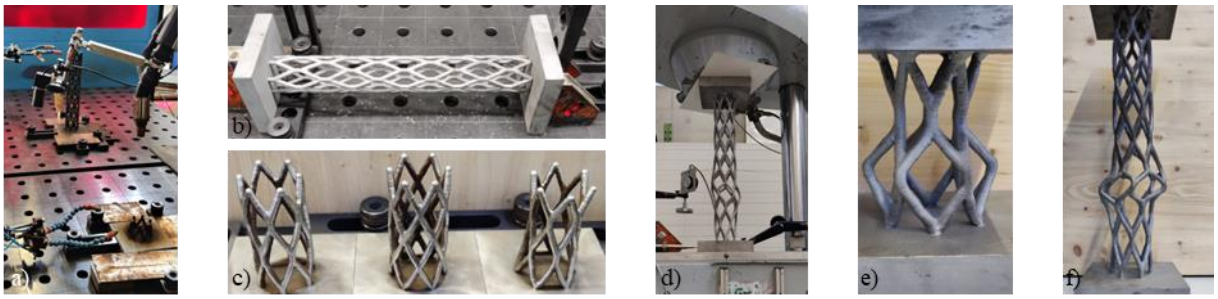

Figure 7: a) Manufacturing process; b) test preparation; c) LS150_HS1, LS150_RS1 and LS150_HP1; d) test-set-up; e) tested LS150_HP1; f) tested LS40_HS1

Table 4: Manufacturing details of the steel lattice strucutres using dot-by-dot printing

		LS150 HS1	LS150 HS2	LS150 HS3	LS150 RS1	LS150 HP1	LS450 HS1	LS450 HS2	LS450 HS3	Sum / Avg*
Lattice shape		hexagon	hexagon	hexagon	rhombus	hexagon	hexagon	hexagon	hexagon	
Colum shape		straight	straight	straight	straight	parabolic	straight	straight	straight	
$\sum$ $Segemnts_{vertical}$	in pcs	3	3	3	0	2	10	10	10	41
$\sum$ $Segemnts_{diagonal}$	in pcs	3	3	3	4	3	10	10	10	46
$\sum$ Dots	in pcs	1188	1188	1044	1200	996	3480	3480	3480	16056
$\sum$ $Dots_{vertical}$	in pcs	144	144	144	0	96	480	480	480	1968
$\sum$ $Dots_{diagonal}$	in pcs	1044	1044	900	1200	900	3000	3000	3000	14088
$H_{structure}$	in mm	151.30	151.15	139.36	144.99	126.49	466.28	467.60	459.28	
$h_{layer,vertical\ strut}$	in mm	1.33	1.33	1.34	-	1.25	1.29	1.30	1.29	1.30*
$h_{layer,diagonal\ strut}$	in mm	1.24	1.24	1.19	1.21	1.18	1.21	1.21	1.19	1.21*
$\sum$ $Dots_{per\ minute}$	in pts/min	6.25	6.25	8.78	8.78	8.78	7.86	7.86	8.78	
$\sum$ $Errors_{process}$	in pcs	8	5	1	1	4	13	4	6	42
$\sum$ $Errors_{structural}$	in pcs	3	0	1	1	0	4	8	3	20

6.2. Load-bearing capacity testing of steel lattice structures

Four different types of columns were tested in an universal testing machine from MAN (maximum load: 1000 kN) under centric compression load (given in Figure 7 d)). The bearing is assumed to be fixed, as inductive displacement transducers were unable to detect any horizontal movement of the plates. The

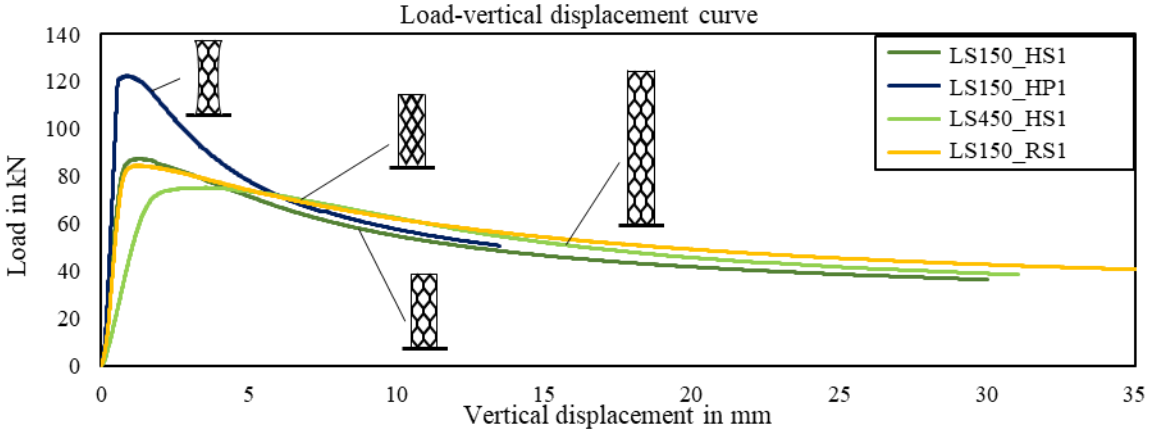

Figure 8: Load-vertical displacement curve of tested lattice structures

test is displacement-controlled, initially at 1 mm/min and then at 5 mm/min once the maximum load has been reached. The results are shown in Figure 8. A load-deformation curve similar to stability failure can be observed for all columns. While the lattice structures of constant cross-section achieve a maximum load bearing capacity of approx. 80 kN, the influence of the parabolic column shape is characterized by a load capacity of 122 kN, which is approx. 1.5 times higher. The main cause of failure is a local failure of the nodes on their underside. For column LS450_HS1, lateral deflection (not in the center of the column) can be detected, which is probably due to local imperfections from manufacturing.

7. Conclusion

The presented findings on the manufacturing of steel lattice structures using dot-by-dot printing of mild carbon steel provide a strong and promising basis for further application in the steel construction industry. This contribution set the focus on understanding the influence of different cooling approaches on material properties which are necessary and of high significance for dot-by-dot printing before presenting first approaches for printed lattice structures. The following conclusions can be drawn based on the discussed results:

- The CMT CS process is suitable for dot-by-dot printing, both for vertical and cantilevered struts.
- The achieved material properties of dot-by-dot printed WAAM-struts indicate material strength equal or higher to the wire electrodes material properties. The recorded strain values substantiate a ductile behaviour under tensile loading.
- The difference between NC and both active cooling approaches (AC and WAC) indicates beneficial effects on material strength.
- While previously the optimization of the lattice column cross-section was only considered by a parabolic shape and without an optimization of the lattice pattern, the result of the tapered cross-section indicates the potential of the possible load increase.

Therefore, the dot-by-dot printing in WAAM using active cooling approaches and optimized cross-section approaches seems to provide great potential for further application into steel lattice structures or other steel structure attempts.

Acknowledgements

We would like to thank the companies Fronius Deutschland GmbH, Messer SE & Co. KGaA and WDI – Westfälische Drahtindustrie GmbH for their kind support.

References

[1] L. Gardner, “Metal additive manufacturing in structural engineering – review, advances, opportunities and outlook,” *Structures*, early access. doi: 10.1016/j.istruc.2022.12.039.
[2] E. Edemskaya and A. Agkathidis, “Rethinking Complexity: Vladimir Shukhov’s Steel Lattice Structures,” *Journal IASS*, vol. 57, no. 3, pp. 201–208, 2016, doi: 10.20898/j.iass.2016.189.806.
[3] S. Norin. “Moscow, Shukhov Tower in February 2014.” [Online]. Available: https://commons.wikimedia.org/wiki/File:Moscow,_Shukhov_Tower_in_February_2014_(12323741925).jpg
[4] D. Kampffmeyer and M. Wolters, “Moderne Schutzgase zum MAG-Schweißen von unlegierten Stählen,” in *DVS Congress 2015: Große Schweißtechnische Tagung, DVS-Studentenkongress ; Fügen von faserverstärkten Kunststoffen, anwendungsnahe Schweißsimulation, Schulung und Prüfung im DVS, IBESS – Forschungscluster „Bruchmechanik“ ; Vorträge der Veranstaltungen im Rahmen von DVS Congress und DVS Expo in Nürnberg vom 15. und 17. September 2015*, Nürnberg, vol. 315, 2015, pp. 249–253.
[5] Y. Bandari, S. Williams, J. Ding, and F. Martina, “Additive manufacture of large structures: robotic or CNC systems?,” in *Proceedings: 26th annual international solid freeform fabrication symposium: - an additive manufacturing conference*, Austin, Texas, University of Texas at Austin, Ed., 2015, pp. 17–25.

[6] F. Martina and S. Williams, "Wire+arc additive manufacturing vs. traditional machining from solid: a cost comparison," Welding Engineering and Laser Processing Centre (WELPC) Cranfield University, Cranfield, 2015. Accessed: May 24, 2023.
[7] J. Müller *et al.*, "Design and Parameter Identification of Wire and Arc Additively Manufactured (WAAM) Steel Bars for Use in Construction," *Metals*, early access. doi: 10.3390/met9070725.
[8] V. Mechtcherine, J. Grafe, V. N. Nerella, E. Spaniol, M. Hertel, and U. Füssel, "3D-printed steel reinforcement for digital concrete construction – Manufacture, mechanical properties and bond behaviour," *Construction and Building Materials*, vol. 179, pp. 125–137, 2018. doi: 10.1016/j.conbuildmat.2018.05.202. [Online]. Available: https://www.sciencedirect.com/science/article/pii/S095006181831287X
[9] K. Tischner *et al.*, "Bond Behavior of WAAM Reinforcements in Comparison to Conventional Steel Reinforcements," *Construction Materials*, early access. doi: 10.3390/constrmater3020014.
[10] I. Ariza, "Adaptive Detailing: Design and Fabrication Methods for In Place Wire and Arc Additive Manufacturing Connection Details," Doctoral Thesis, Institut für Technologie in der Architektur, Eidgenössische Technische Hochschule Zürich, Zürich, 2022. [Online]. Available: https://www.research-collection.ethz.ch/handle/20.500.11850/602129
[11] V. Laghi, M. Palermo, G. Gasparini, and T. Trombetti, "Computational design and manufacturing of a half-scaled 3D-printed stainless steel diagrid column," *Additive Manufacturing*, vol. 36, p. 101505, 2020, doi: 10.1016/j.addma.2020.101505.
[12] T. Abe and H. Sasahara, "Layer geometry control for the fabrication of lattice structures by wire and arc additive manufacturing," *Additive Manufacturing*, early access. doi: 10.1016/j.addma.2019.06.010.
[13] R. Dörrie *et al.*, "Combined Additive Manufacturing Techniques for Adaptive Coastline Protection Structures," *Buildings*, early access. doi: 10.3390/buildings12111806.
[14] V.-A. Silvestru *et al.*, "Performance under tensile loading of point-by-point wire and arc additively manufactured steel bars for structural components," *Materials & Design*, early access. doi: 10.1016/j.matdes.2021.109740.
[15] L. J. Da Silva, D. M. Souza, D. B. de Araújo, R. P. Reis, and A. Scotti, "Concept and validation of an active cooling technique to mitigate heat accumulation in WAAM," *Int J Adv Manuf Technol*, vol. 107, 5-6, pp. 2513–2523, 2020. doi: 10.1007/s00170-020-05201-4. [Online]. Available: https://link.springer.com/article/10.1007/s00170-020-05201-4
[16] U. Reisgen, R. Sharma, S. Mann, and L. Oster, "Increasing the manufacturing efficiency of WAAM by advanced cooling strategies," *Weld World*, vol. 64, no. 8, pp. 1409–1416, 2020, doi: 10.1007/s40194-020-00930-2.
[17] T. Feucht, J. Lange, B. Waldschmitt, A.-K. Schudlich, M. Klein, and M. Oechsner, "Welding Process for the Additive Manufacturing of Cantilevered Components with the WAAM," in *Advanced Joining Processes* (Advanced Structured Materials), L. F. M. Da Silva, P. A. F. Martins, and M. S. El-Zein, Eds., Singapore: Springer Singapore, 2020, pp. 67–78.
[18] F. R. Teixeira, F. M. Scotti, V. L. Jorge, and A. Scotti, "Combined effect of the interlayer temperature with travel speed on features of thin wall WAAM under two cooling approaches," *Int J Adv Manuf Technol*, early access. doi: 10.1007/s00170-023-11105-w.
[19] P. Henckell, K. Günther, Y. Ali, J. Bergmann, J. Scholz, and P. Forêt, "The Influence of Gas Cooling in Context of Wire Arc Additive Manufacturing—A Novel Strategy of Affecting Grain Structure and Size," in *TMS 2017 146th Annual Meeting & Exhibition Supplemental Proceedings*, The Minerals, Metals & Materials Society TMS, Ed., 2017, pp. 147–156, doi: 10.1007/978-3-319-51493-2_15.
[20] T. Feucht, M. Erven, B. Waldschmitt, J. Lange, and D. Kampffmeyer, "Einfluss des Schutzgases auf auskragend gefertigte WAAM-Strukturen," in *DVS Congress 2021. Große Schweißtechnische Tagung DVS CAMPUS*, Essen, DVS - Deutscher Verband für Schweißen und verwandte Verfahren e. V., Ed., vol. 371, 1st ed., 2021, pp. 301–307.
[21] T. Feucht, J. Lange, M. Erven, C. B. Costanzi, U. Knaack, and B. Waldschmitt, "Additive manufacturing by means of parametric robot programming," *Construction Robotics*, vol. 4, 1-2, pp. 31–48, 2020, doi: 10.1007/s41693-020-00033-w.